An Urban Water Extraction Method Combining Deep Learning and Google Earth Engine

Yudie Wang, Zhiwei Li, Chao Zeng, Gui-Song Xia, *Senior Member, IEEE*, and Huanfeng Shen, *Senior Member, IEEE*

***Abstract*—Urban water is important for the urban ecosystem. Accurate and efficient detection of urban water with remote sensing data is of great significance for urban management and planning. In this article, we proposed a new method by combining Google Earth Engine (GEE) with a multiscale convolutional neural network (MSCNN) to extract urban water from Landsat images, which can be summarized as "offline training and online prediction" (OTOP). That is, the training of MSCNN is completed offline, and the process of urban water extraction is implemented on GEE with the trained parameters of MSCNN. The OTOP can give full play to the respective advantages of GEE and the convolutional neural network (CNN), and can make the use of deep learning method in GEE more flexible. The proposed method can process the available satellite images with high performance, without data download and storage, and the overall performance of urban water extraction in the test areas is also higher than that of the modified normalized difference water index (MNDWI) and random forest classifier. The results of the extended validation in the other major cities of China also showed that OTOP is robust and can be used to extract different types of urban water, which benefits from the structural design and training of MSCNN. Therefore, OTOP is especially suitable for the study of large-scale and long-term urban water change detection in the background of urbanization.**

***Index Terms*—Convolutional neural network, google earth engine, urban water, water extraction.**

I. Introduction

URBAN water is a significant part of the urban ecosystem and plays an important role in human life and urban economic development, such as water supply, flood control, tourism, and urban heat island regulation [1], [2]. Urban water types include rivers flowing through urban areas, and natural or man-made lakes, ponds, and reservoirs. However, in recent decades, due to the impact of human activities and global climate change, land use/cover in urban areas has undergone severe changes, resulting in dramatic changes in the distribution and abundance of urban water [3], [4]. This not only hinders the sustainable development of urban water resources, but also affects the normal function of the urban ecosystems [5]. Therefore, an objective and accurate understanding of the spatio-temporal distribution characteristics of urban water is essential for urban planning and development.

Satellite remote sensing technology has been widely used in the mapping of water, because of its wide range of observations and relatively low cost [6], [7]. Previous studies have proposed many methods for water extraction from satellite images. The water index methods are extensively used because of their easy implementation and high computational efficiency. Examples of such water indices are the normalized difference water index (NDWI) [8], the modified normalized difference water index (MNDWI) [9], and the automatic water extraction index (AWEI) [10]. These water indices can enhance the water information based on the spectral reflectance characteristics of water in the visible and infrared bands. However, it is difficult to determine the optimal thresholds for different images to effectively distinguish between water and non-water, because the spectral characteristics of water vary both spatially and temporally [11]. Furthermore, for urban water extraction, these indices also have the problem of easily confusing urban water with low-albedo non-water surfaces, such as asphalt roads and building shadows [10].

Many machine learning methods can also be used to extract urban water from satellite images, to improve the classification accuracy, such as maximum likelihood estimation (MLE) [12], [13], support vector machine (SVM) [14]–[16], and random forest [17]–[19]. Most of these methods can effectively learn the characteristics of water and can distinguish it from other objects in the case of accurate training samples. However, in addition to being reliant on high-quality training data, it is also necessary to select appropriate combinations of features for these methods, which may include spectral, textural, and shape features, especially in urban areas. The feature selection directly affects the stability of the prediction, and the design of the features is not only time-consuming and laborious, but also requires rich prior experience to make up for the shortcomings of the data mining.

Manuscript received November 7, 2019; revised January 18, 2020; accepted January 29, 2020. Date of publication February 10, 2020; date of current version September 18, 2020. This work was supported by the National Key R&D Program of China under Grant 2018YFA06055. *(Corresponding author: Huanfeng Shen.)*

Yudie Wang is with the State Key Laboratory for Information Engineering in Surveying, Mapping, and Remote Sensing (LIESMARS), Wuhan University, Wuhan 430079, China (e-mail: ydiewang@whu.edu.cn).

Zhiwei Li and Chao Zeng are with the School of Resource and Environmental Sciences, Wuhan University, Wuhan 430079, China (e-mail: lizw@whu.edu.cn; zengchaozc@hotmail.com).

Gui-Song Xia is with the School of Computer Science and the State Key Laboratory of Information Engineering in Surveying, Mapping and Remote Sensing (LIESMARS), Wuhan University, Wuhan 430079, China (e-mail: guisong.xia@whu.edu.cn).

Huanfeng Shen is with the School of Resource and Environmental Sciences, Wuhan University, Wuhan 430079, China, and also with the Collaborative Innovation Center of Geospatial Technology, Wuhan University, Wuhan 430079, China (e-mail: shenhf@whu.edu.cn).

Digital Object Identifier 10.1109/JSTARS.2020.2971783

As a subset of machine learning, deep learning, and especially convolutional neural networks (CNNs), has also demonstrated its effectiveness in image processing in recent research [20]–[22]. The greatest advantage of CNNs is their strong ability to extract multiscale and multilevel features. Some scholars have used CNNs to extract water from different types of images, and the results showed that CNNs can accurately distinguish between water and ice/snow, cloud shadows, and terrain shadows, without additional auxiliary materials [23]–[26]. However, most of these studies were of small-scale or short-term. For large-scale and long-term urban water extraction, the download and storage of massive satellite images and the requirement for high computational performance are unavoidable challenges.

Google Earth Engine (GEE) is a cloud platform dedicated to geographic data processing and analysis, which can be used to solve these problems. GEE provides massive global geospatial data and many excellent image-processing algorithms, and all the processing is parallel [27], [28]. These advantages enable researchers to perform large-scale and long-term analysis with minimal cost and equipment [29]–[33], including surface water mapping [34]–[37]. However, to date, the function of deep learning on GEE is still developing. The existing research on the combination of GEE and deep learning has mainly used GEE as the data source or as a platform for creating training and test datasets, whereas the training and testing of the deep learning models were undertaken on other platforms [38]–[40]. However, this approach does not fully utilize the advantages of GEE, which is designed specifically for managing big data.

Therefore, in this article, we propose a new method by combining GEE with a CNN model to detect urban water. The completed CNN model, which is called the multiscale convolutional neural network (MSCNN), is trained offline using selected Landsat images and the corresponding water masks. The trained model parameters are uploaded to GEE and used to simulate the process of MSCNN's urban water detection to complete the urban water extraction of Landsat images on GEE. The proposed framework can be summarized as "offline training and online prediction" (OTOP). The goal of the OTOP method is to provide a more flexible way to combine the preferred deep learning model and GEE. The proposed framework can make full use of the high-precision advantage of CNNs and the massive data storage and powerful data-processing abilities of GEE, so as to achieve efficient and accurate urban water detection and provide technical support for long-term, large-scale research.

II. Experimental Data and Areas

A. Experimental Data

Based on the advantages of the relatively high spatial resolution (30 m) and long observation records (1972 to the present), Landsat data have become one of the most commonly used data types for monitoring the long-term changes of water [41]–[46]. The Landsat surface reflectance (SR) data on GEE were selected to ensure the consistency of the data. The Landsat Thematic Mapper (TM) and Enhanced Thematic Mapper Plus (ETM+) SR data were generated from the Landsat standard Level 1 Terrain-corrected (L1T) images from the USGS archives with the Landsat Ecosystem Disturbance Adaptive Processing System (LEDAPS) algorithm [47], and the Landsat Operational Land Imager (OLI) SR data from the USGS archives were processed with the Landsat Surface Reflectance Code (LaSRC) algorithm [48].

The characteristics of urban water vary, due to the diversity of the urban terrain and urban development plan. In order to ensure the strong generality and robustness of the OTOP method, the selection of training data needed to consider as many cases as possible. Therefore, in this article, 36 Landsat images covering 36 major cities in China, most of which are provincial capitals and municipalities, were chosen as the experimental data. These 36 cities basically represent the situations of urban water under the different climate, topography, and development levels in China. The 36 images we used were acquired at different times and came from three different sensors: Landsat TM, ETM+, and OLI. These images also covered many different surface features. In addition, cloudy images were also included in the experimental data, because the effects of clouds and cloud shadows are inevitable in the real world. In order to increase the differentiation between water and the other objects in urban areas, the sample size of the urban areas was appropriately increased in the training data. Therefore, the CNN model trained by the dataset selected under the multiple considerations could be used for the extraction of urban water in different cities of China at different times. The spatial distributions and acquisition times of the selected images are shown in Fig. 1 and Table I.

The water masks of the 36 selected Landsat images were manually drawn by referring to the original images and the high-resolution images of the same periods on Google Earth. The mapping of the water masks followed uniform standards, including: 1) the water bodies of less than 4 pixels were not delineated; 2) it is not easy to determine the slender water bodies with a width of less than 2 pixels, so these were ignored; and 3) according to actual experience, the mixed pixels located at the edges of water areas were identified as water if the water features were obvious, otherwise as non-water. Finally, the manually labeled reference water masks were created by setting the pixel values of water and non-water to 1 and 0, respectively.

B. Test Areas

For the accuracy verification of the OTOP method for urban water extraction, we chose the central urban areas of Changchun, Wuhan, Kunming, and Guangzhou as the test areas. The extents of the central urban areas were determined by the latest urban planning records for each city.

Changchun is located in the Northeast Plain of China, and the water in the territory is mainly tributaries of rivers. Wuhan, located in the Jianghan Plain in Central China, is dotted with nearly a hundred lakes, and is known as the "city of a hundred lakes". Kunming is located in the middle of the Yunnan-Guizhou Plateau in Southwestern China, where most of the water bodies are plateau lakes and reservoirs. Guangzhou is a coastal city, located

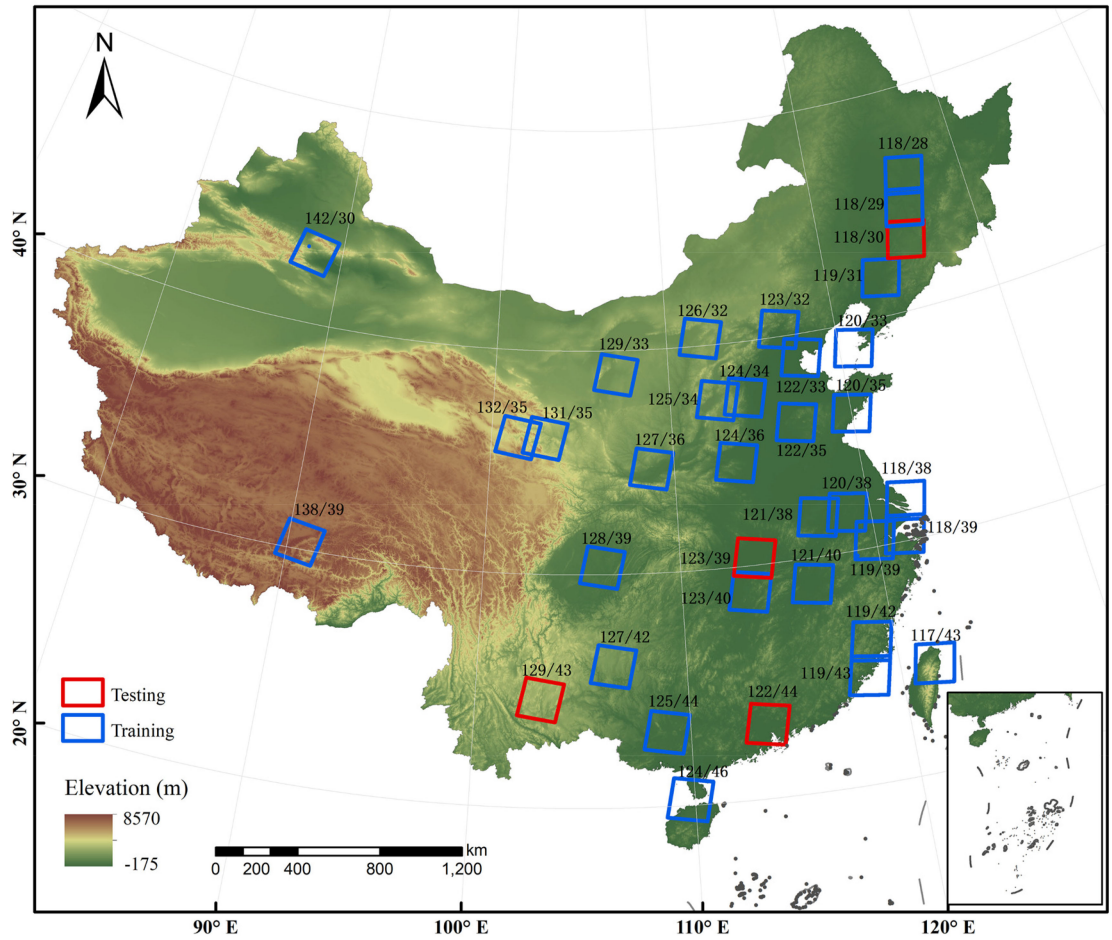

Fig. 1. Spatial distribution of the experimental data from China. The blue and red boxes represent the spatial locations of the images used for training and testing in the accuracy assessment, respectively.

TABLE I
WRS-2 PATH/ROW, THE ACQUISITION TIME AND THE CORRESPONDING CITIES OF LANDSAT TM, ETM+, AND OLI IMAGES USED IN THIS ARTICLE

Sensor	Path/row	Date	City	Sensor	Path/row	Date	City	Sensor	Path/row	Date	City
ETM+	117/043	March 6, 2001	Taipei	TM	120/038	December 8, 2004	Nanjing	ETM+	125/034	November 20, 1999	Taiyuan
TM	118/028	May 14, 2009	Harbin	TM	121/038	September 2, 1995	Hefei	TM	125/044	March 3, 1994	Nanning
ETM+	118/029	April 11, 2000	Jilin	OLI	121/040	September 9, 2015	Nanchang	OLI	126/032	February 5, 2017	Hohhot
OLI	118/030	April 13, 2015	Changchun	OLI	122/033	May 13, 2016	Tianjin	TM	127/036	June 8, 1995	Xian
TM	118/038	April 20, 2006	Shanghai	OLI	122/035	November 29, 2013	Jinan	TM	127/042	May 19, 2011	Guiyang
TM	118/039	February 9, 1998	Ningbo	TM	122/044	November 23, 2005	Guangzhou	OLI	128/039	August 6, 2014	Chongqing
TM	119/031	August 24, 1991	Shenyang	ETM+	123/032	June 4, 2001	Beijing	TM	129/033	July 1, 2010	Yinchuan
TM	119/039	October 1, 1999	Hangzhou	TM	123/039	April 9, 1995	Wuhan	ETM+	129/043	February 20, 2000	Kunming
TM	119/042	January 8, 2007	Fuzhou	TM	123/040	September 24, 2004	Changsha	TM	131/035	May 30, 2005	Lanzhou
TM	119/043	January 28, 1997	Xiamen	TM	124/034	October 2, 2010	Shijiazhuang	TM	132/035	November 7, 1997	Xining
TM	120/033	February 3, 2008	Dalian	TM	124/036	October 16, 1992	Zhengzhou	TM	138/039	November 18, 2003	Lhasa
TM	120/035	May 8, 1996	Qingdao	OLI	124/046	June 26, 2015	Haikou	ETM+	142/030	October 18, 2002	Urumqi

The significance of bold entities in Table II is the best result in the accuracy assessment.

in a hilly area, with a developed river system and a vast water area. These four cities cover all the main types of urban water, with different depths, turbidities, and surface morphologies. The spectral features of the built-up areas of the four cities are also different, covering most of the major challenges affecting the extraction of urban water, such as building shadows, low-albedo roofs, and roads. The images of the four cities used for the testing were also from different sensors. Thus, the accuracy assessment of the urban water extraction in these four cities could adequately reflect the ability of the OTOP method. In the

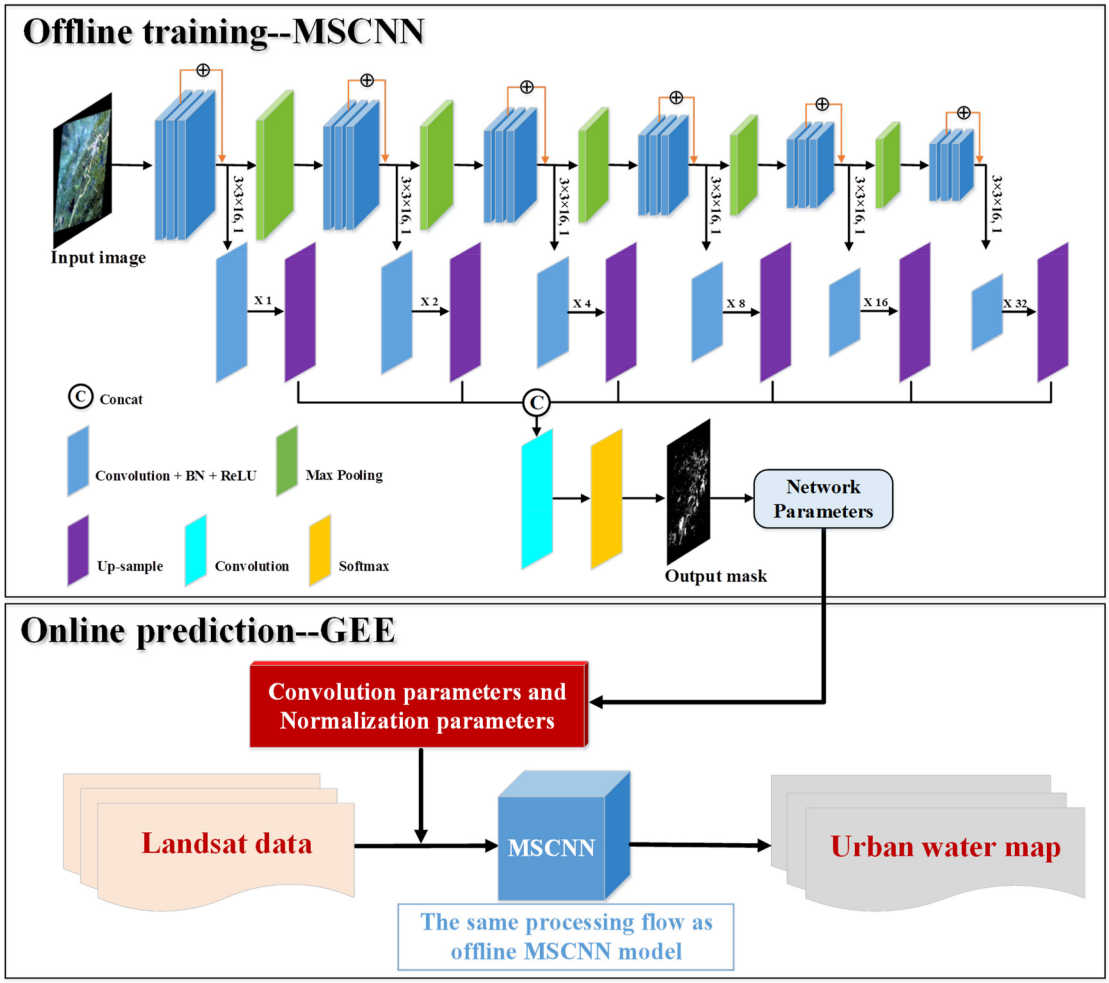

Fig. 2. Flow chart of the OTOP framework.

experiment, the data of the other 32 cities were used for the model training.

III. Methodology

The flow chart of the proposed OTOP framework is shown in Fig. 2. The framework is divided into two main parts: 1) offline training with MSCNN, and 2) online prediction on GEE. Details of the different components are provided in the following sections.

A. Offline Training

1) Data Preparation: The training data and test data consisted of Landsat TM/ETM+/OLI SR images and the corresponding water masks which were manually created. To better eliminate the interference of building shadows in the water extraction, the training data included not only the images and water masks of the 32 cities, but also the data of the built-up areas in these images.

The input of the network model was the three visible bands, the near-infrared band, and the two short-wave infrared bands of Landsat imagery. The pixel values of the SR images were first unified to the range of [0, 1] by dividing by 10 000 before the data were used for the model training. In the online prediction stage, the Landsat images were processed in the same way as the training stage. Then, before training the model, a moving window was used to clip the large multispectral images and masks to pairs of nonoverlapping training samples with a height and width of 256 × 256 pixels. Finally, more than 30 000 pairs of image blocks were used for the model training.

2) Multiscale CNN Model: As shown in Fig. 2, the CNN model used in the offline training, which is called MSCNN, is implemented with reference to the multiscale convolutional feature fusion (MSCFF) model proposed by Li *et al.* [49]. The MSCFF model was designed for the cloud/cloud shadow detection of multisource remote sensing images, and its advantages are obvious when compared with the traditional rule-based methods and the existing deep learning models. Considering that the deep learning method is universal in image classification, and that urban water extraction and cloud/cloud shadow detection are both classification problems, the MSCNN model was designed for the urban water extraction. The complex encoder–decoder module of MSCFF was simplified in the MSCNN model, under the comprehensive consideration of the model accuracy and computational efficiency. In addition, the MSCFF module was

used in the MSCNN model to further improve the accuracy of urban water extraction by making full use of the convolutional features of different scales.

The MSCNN model is made up of convolution operations at six different scales. At each scale, the image is processed by three multifeature convolution operation layers and a single-feature convolution operation layer, which is used to extract higher level feature information and reduce the channels of the feature maps. Except for the final scale, the last multifeature convolutional layer of each scale is followed by a pooling layer that reduces the spatial dimensions of the input data while ensuring the translational invariance of the feature extraction. A max-pooling operation with 2×2 filters and a two-pixel stride is used, which returns the maximum value for each window. The six single-feature maps of different scales are sampled to the same size as the input data, and the upsampling results are aggregated as the input of the last convolutional layer. This multiscale feature fusion can provide a broad description of the context of the given spatial locations [23]. The upsampling operation in MSCNN is directly implemented by bilinear interpolation. The output of the last convolutional layer of the network is processed by the softmax layer to output the class probability map of water and non-water. The class with the highest probability is then regarded as the final classification result.

Moreover, in the MSCNN model, each convolutional layer, except for the last one, is followed by a batch normalization (BN) layer and a rectified linear unit (ReLU, $f(x) = \max(0, x)$). The BN layer can speed up the training of the network and avoid the problem of gradient disappearance. ReLU, as a nonlinear activation function, can introduce nonlinear factors into the network and ensure that the parameters can continue to converge. The convolutional kernel size of each convolutional layer is 3×3, and the output feature maps of each layer are kept the same size as the input data by adding zeros at the image borders in the convolution operation. Cross-entropy loss is used as the loss function in this model, to measure the differences between the predicted and the expected results, which can be calculated as follows:

$$\text{loss} = -\frac{1}{N}\sum_{x=i}^{x=N}\left[y_i \ln F\left(x_i, w\right) + \left(1 - y_i\right)\ln\left(1 - F\left(x_i, w\right)\right)\right] \tag{1}$$

where x_i is the input, y_i is the expected output, $F(x_i, w)$ is the actual output, and N is the number of training samples.

In the training process, stochastic gradient descent (SGD) and back-propagation (BP) are used to update the weight parameters w until the optimal parameters are obtained by minimizing the loss function. The initial learning rate of the model is set to 0.1, and the learning rate follows the polynomial decay from 0.1 to 0 before the maximum number of iterations (200 000) is reached. Finally, the optimal weight parameters of the model are stored and then uploaded to GEE for online urban water detection.

B. Online Prediction

The most important step when extracting the extent of urban water on GEE is to simulate the process of water detection for the offline MSCNN model with the uploaded trained parameters. As mentioned above, the training processes in the MSCNN model are mainly composed of convolutional operations, max pooling, upsampling operations, and basic arithmetic operations of the images. These basic operations are implemented one by one in GEE, and then integrated according to the framework of the MSCNN model to realize the extraction of urban water using the CNN model on the cloud platform.

The GEE platform provides many basic encapsulated algorithms while providing users with an online JavaScript API that allows them to create and run custom algorithms. GEE supports a variety of complex geospatial analysis operations, including image classification, change detection, and time-series analysis [50]. In addition, users can upload charts and raster or vector data to GEE for processing, and our research makes full use of the characteristic. The convolutional operations and image algebra operations of the MSCNN model can be implemented directly on GEE. The parameters of the convolutional kernels also support user-definition, so the kernel of each convolutional operation can be defined with the uploaded parameters of MSCNN. The process of max-pooling is equivalent to downsampling, and GEE provides reduction and reprojection operations to change the image resolution. Similarly, the upsampling process can also be directly achieved by reprojection and resampling (bilinear interpolation) on GEE. The results of the urban water extraction code implemented by simulating MSCNN on GEE are the same as the offline results, i.e., the maximum probability class map. Based on the results, the final water extent can be determined.

IV. Results

There were two parts in the verification of the feasibility and robustness of the OTOP method. The first part was the accuracy assessment of the method, where the predicted results of OTOP were compared with the urban water extraction results of other methods. The second part was to apply the OTOP method to other major cities in China and evaluate the accuracy. The specific results are provided in the following sections.

A. Accuracy Assessment

1) Compared Methods: The OTOP method was compared with two typical methods — the traditional MNDWI method [9] and the RF method [51] — to prove the effectiveness of the combination of GEE and MSCNN in urban water extraction. The threshold of each MNDWI image is automatically determined by the Otsu method [52]. However, due to the threshold shifting problem of the Otsu method [53], an additional condition for determining the final threshold is added through the approximate statistics of the MNDWI values of water pixels in all experimental data. That is, when the threshold detected by the Otsu method is less than 0.05, the threshold will be directly set to 0.05, and when it is greater than 0.05, the threshold detected by the Otsu method will be selected as the final threshold. Furthermore, the RF algorithm has already been encapsulated on the GEE platform. The six bands of the Landsat images and the two texture features of variance and contrast were selected as feature variables of RF. The addition of texture features obtained

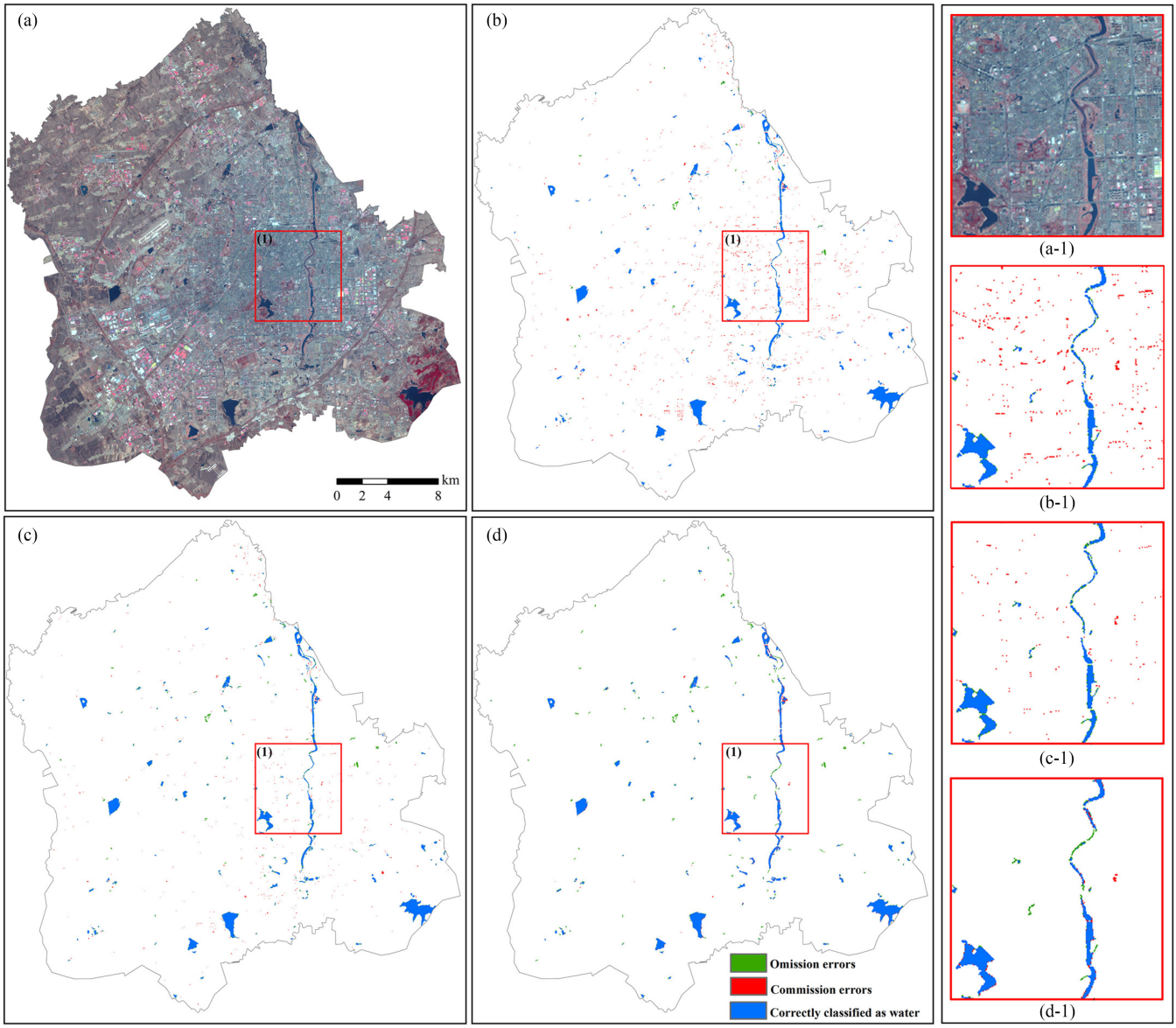

Fig. 3. Comparison of the urban water extraction results for Changchun. (a) NIR-R-G false-color display of the original Landsat image of the central urban area of Changchun. (b)–(d) Results of urban water mapping with MNDWI, RF, and OTOP, respectively. Blue color in (b)–(d) shows the accurately detected urban water bodies, the green shows the missing urban water bodies, and the red shows the false detection. The colors in Figs. 4–7 have the same meanings.

from the gray-level co-occurrence matrix [54] enabled RF to also utilize the spatial information of the image. The training samples of RF were the same as for the MSCNN model. The number of classification trees was determined to be 40 by comparative experiments, because the performance of RF was not substantially improved when greater than 40. It is worth noting that both MNDWI and the RF method can be directly implemented on GEE, in order to compare the difference between OTOP and the pure online methods in the extraction of urban water.

2) Urban Water Extraction Maps: Urban water extraction maps of the central urban areas of Changchun, Wuhan, Kunming, and Guangzhou generated by MNDWI, RF, and the OTOP method are shown in Figs. 3–6. On the whole, all the methods can accurately extract evident and clear urban water bodies, such as large rivers, lakes, reservoirs, and ponds. However, compared with MNDWI and RF, the OTOP method performs better in the presence of complex urban surfaces. For the urban centers with dense buildings, in particular, the OTOP method can more accurately distinguish water from other non-water objects in the four test cities.

Visually, the traditional MNDWI shows the most serious case of misclassifying building shadows as water in the urban water extraction results. There are different degrees of false detection in the four cities, which is the most obvious in Guangzhou, where there are dense high-rise buildings (Fig. 7). It is difficult to distinguish building shadows and low-albedo objects from water using a threshold because they have similar index values. The results of RF show some improvement over those of MNDWI. However, RF also has the same problem of false detection in urban areas. This indicates that the accuracy of RF is also

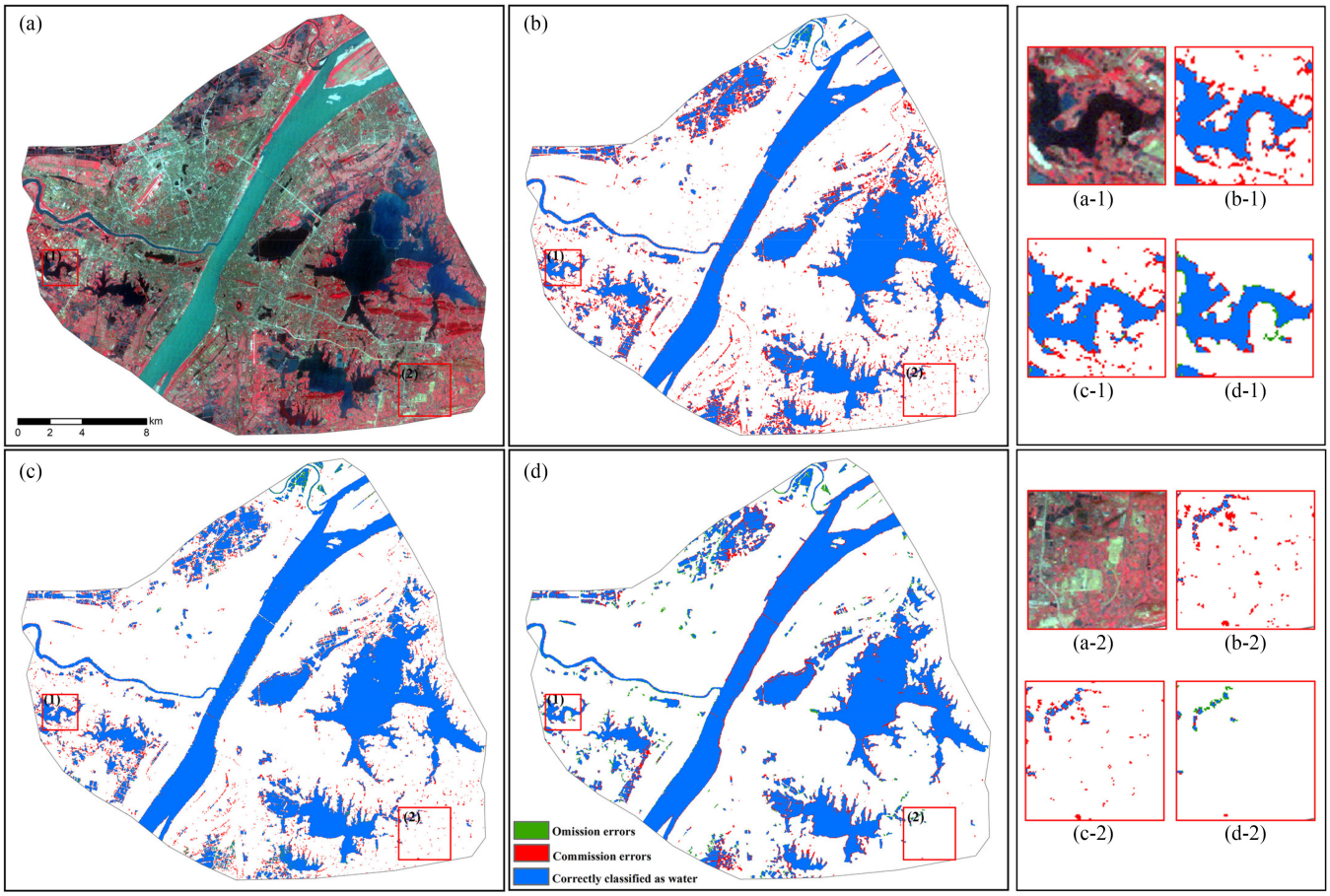

Fig. 4. Comparison of the urban water extraction results for Wuhan. (a) NIR-R-G false-color display of the original Landsat image of the central urban area of Wuhan. (b)–(d) Results of the urban water mapping with MNDWI, RF, and OTOP, respectively.

inferior to the proposed OTOP method when the same training samples were used and the spectral and spatial characteristics of water were also considered. Furthermore, the performance of RF is unstable in the different cities. For example, the false detection of RF is more obvious in Guangzhou, but there are also obvious missing detections in the extraction of urban water in Kunming, some of which even occur in the center of water bodies [Fig. 4(c-2)]. This indicates that RF is not robust enough for water extraction in different areas, and it is more suitable for urban water extraction at a regional scale. Moreover, MNDWI and RF also show obvious errors around the lakes within the central area of Wuhan. Most of these areas are vegetated farmland or small water bodies that are mixed with other objects, due to the spatial resolution of Landsat. MNDWI and RF can identify these as water, indicating that these two methods are sensitive to water signals.

Relatively speaking, in the four test cities, the OTOP method performs well in both false detections and missing detections, both of which are within acceptable limits. This is because the MSCNN model trained offline can use the spectral and spatial information of the image to learn the characteristics of water bodies at multiple scales and levels, so as to determine the extent of urban water more accurately. In addition, since there are fewer water areas in Changchun, the extraction results of the RF and OTOP are visually similar. However, a closer observation shows that there are still a few false detections in the results of RF in the urban centers. Compared with RF, the OTOP method improves the accuracy of water extraction in the building areas.

3) Urban Water Extraction Accuracy: The confusion matrix was obtained by comparing the predicted results and the reference masks, pixel by pixel. Five indicators were calculated based on the confusion matrix to quantitatively evaluate the accuracy of the urban water extraction: omission error (OE), commission error (CE), kappa coefficient (kappa), F1-score, and intersection over union [IoU, (2)]. Note that kappa, F1-score, and IoU are comprehensive indicators of the overall performance of a certain method, where a larger value means a higher accuracy, whereas the smaller the OE and CE values, the better the accuracy.

$$\text{IoU} = \frac{\text{Intersection areas of predicted and reference water}}{\text{Union areas of predicted and reference water}}. \tag{2}$$

The accuracies of MNDWI, RF, and the OTOP method for extracting urban water in the four test cities are summarized in Table II. The statistical results show that, among the three methods, the OTOP method achieves a higher accuracy in water extraction at all the test cities. The mean kappa, mean F1-score,

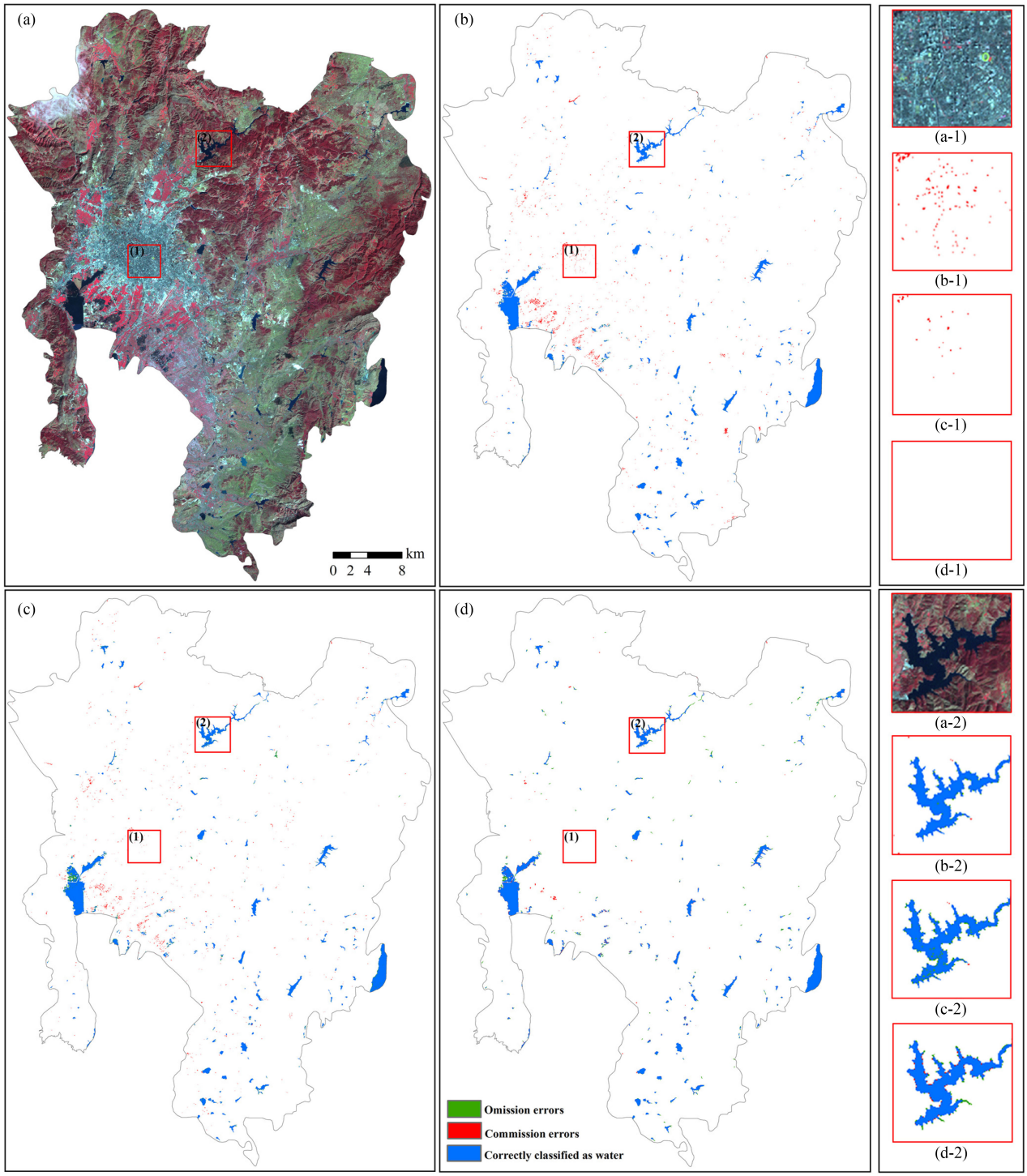

Fig. 5. Comparison of the urban water extraction results for Kunming. (a) NIR-R-G false-color display of the original Landsat image of the central urban area of Kunming. (b)–(d) Results of the urban water mapping with MNDWI, RF, and OTOP, respectively.

and mean IoU of urban water extraction with the OTOP method in the four cities reaches 0.924, 0.930, and 0.869, respectively, which are the highest among the methods. Consistent with the results of the visual inspection, MNDWI shows overestimation in the four test cities, i.e., the false detection is serious. The OEs of MNDWI in Guangzhou and Wuhan are about 1%, but the CEs are high, so the three comprehensive indicators are lower. In Kunming, where the area with dense buildings is relatively small, the false detection of MNDWI is slightly better, the CE is 11.06%, and the OE is 3.60%. The three comprehensive indicators are also relatively high. Compared with MNDWI, the accuracy of RF shows a certain degree of improvement. Except for Kunming, the overall accuracy of urban water extraction with RF in the other three cities is improved, the CE of each

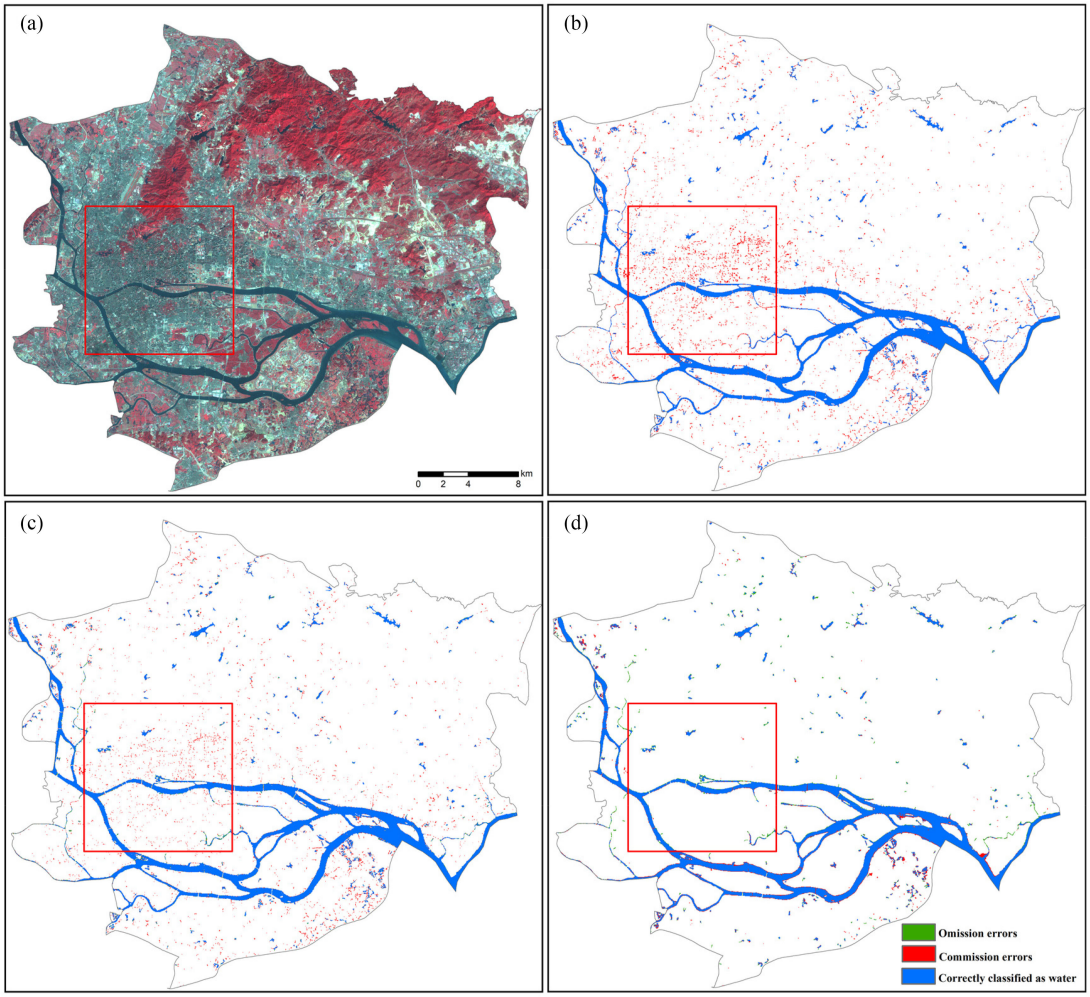

Fig. 6. Comparison of the urban water extraction results for Guangzhou. (a) NIR-R-G false-color display of the original Landsat image of the central urban area of Guangzhou. (b)–(d) Results of the urban water mapping with MNDWI, RF, and OTOP, respectively.

TABLE II
ACCURACY ASSESSMENT RESULTS FOR THE URBAN WATER EXTRACTION AT THE FOUR TEST CITIES BY MNDWI, RF, AND OTOP

Test area	Method	Omission error	Commission error	Kappa	F1-score	IoU
Changchun	MNDWI	8.55%	17.62%	0.864	0.866	0.765
	RF	14.03%	7.64%	0.889	0.890	0.803
	OTOP	14.38%	5.30%	**0.901**	**0.900**	**0.817**
Wuhan	MNDWI	1.29%	17.98%	0.856	0.894	0.808
	RF	4.63%	11.31%	0.893	0.919	0.850
	OTOP	3.76%	9.74%	**0.912**	**0.934**	**0.877**
Kunming	MNDWI	3.60%	11.06%	0.923	0.925	0.860
	RF	7.54%	8.50%	0.918	0.920	0.852
	OTOP	8.85%	4.43%	**0.932**	**0.933**	**0.875**
Guangzhou	MNDWI	0.58%	19.33%	0.885	0.893	0.807
	RF	3.11%	13.73%	0.903	0.910	0.836
	OTOP	6.45%	10.10%	**0.912**	**0.917**	**0.847**
Average of the four test areas	MNDWI	1.16%	17.95%	0.890	0.896	0.812
	RF	7.40%	10.21%	0.902	0.911	0.836
	OTOP	5.18%	8.74%	**0.924**	**0.930**	**0.869**

The significance of bold entities in Table II is the best result in accuracy assessment.

city is decreased, but the OE is inevitably increased. The OE of Changchun, which is 14.03%, increases the most. However, the CEs of RF are higher in Guangzhou and Wuhan with complex urban surfaces, at 11.31% and 13.73%, respectively. On the whole, the quantitative evaluation results for RF also show that although the overall accuracy of urban water extraction is improved, the extraction results in the different cities are quite different. The result of water extraction by RF in Kunming is not even as good as that of MNDWI. Therefore, the RF method is not stable enough for automated large-scale and long-term studies. Compared with these methods, the OTOP method performs better at all the test cities. In addition to the obvious increase

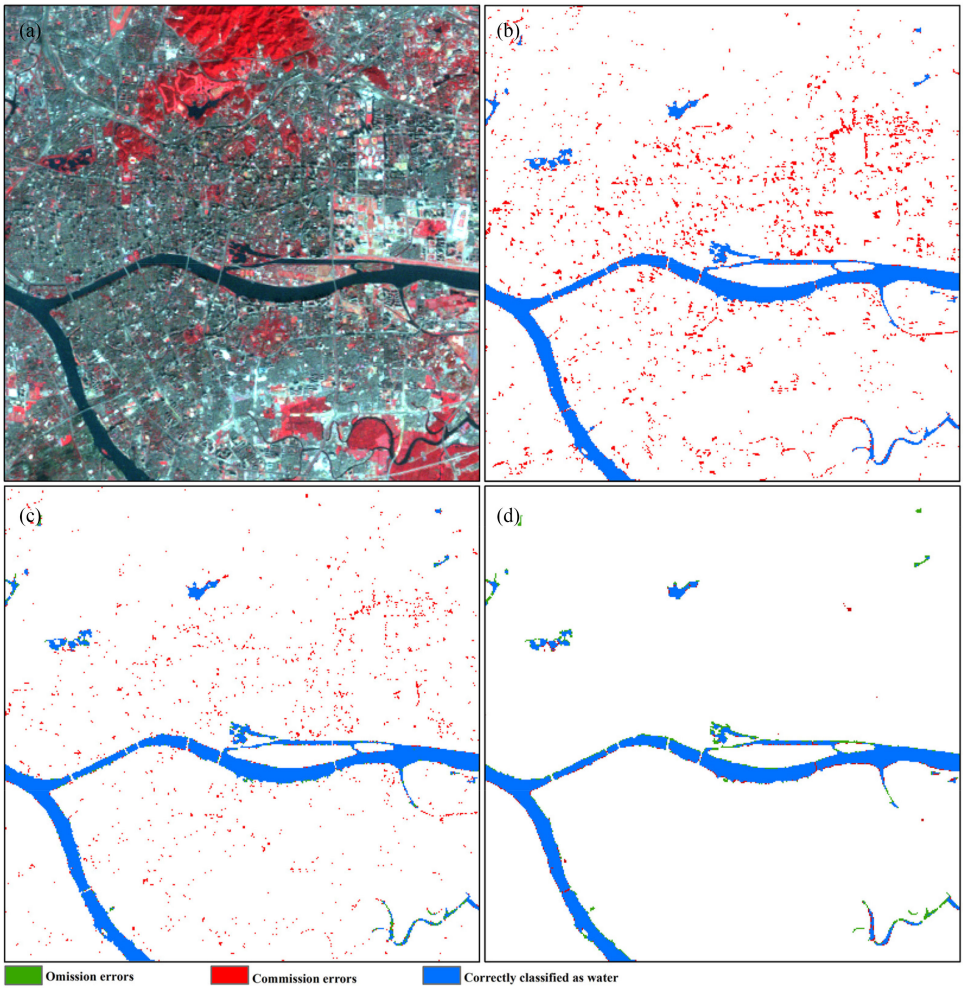

Fig. 7. Details of the water extraction in the dense building area of Guangzhou. (a) NIR-R-G false-color display of the original Landsat image. (b)–(d) Results of urban water mapping with MNDWI, RF, and OTOP, respectively.

of the three comprehensive indicators, the OEs and the CEs of the four cities are also lower values, mostly below 10%. The only larger error is the OE for Changchun, which is 14.38%. However, compared with RF, it can be seen that the OTOP method reduces the CE while reducing the OE as far as possible, because the CE and the OE were mutually constrained. The results for the other cities also show that the OTOP method can achieve a better relative balance between the two indicators of CE and OE. That is to say, the OTOP method not only reduces the problem of CEs in urban areas, but also guarantees as much as possible that there are not many OEs so as to achieve a satisfactory classification accuracy.

Furthermore, from the perspective of overall performance, the OTOP method shows the least difference, compared with the other two methods, in images covering the different test cities and from different sensors. The IoUs of the OTOP method are stable at higher values, and the kappa and F1-score are both above 0.9. This also shows that the OTOP method has strong robustness, and that it can accurately distinguish between water and non-water in urban areas.

B. *Extended Validation in Major Cities of China*

To further demonstrate the universality of the OTOP method, we applied the OTOP method to 32 other major cities in China, and evaluated the accuracy. According to the spatial distribution and development level of each city, the 32 cities were divided into eight groups, without repetition, with four cities in each group. There were nine groups in total, including the previous four cities used for the validation. The Landsat images and water masks of any eight groups were used as training data to extract the urban water in the central urban areas of the remaining four cities. The above operation was repeated eight times, to complete the extended validation of the OTOP method in China. The same five indicators were again used to quantitatively assess the accuracy of the urban water extraction in each city (Fig. 8).

The results of the extended validation show that the OTOP method performs well throughout China, with strong universality. The kappa, F1-score, and IoU for most cities are above 0.9, 0.9, and 0.82, respectively. The OE and CE of the urban water extraction in each city also reach a satisfactory relative balance under the premise of mutual checks and balances. The OEs and CEs of most cities are below 13% and 10%, respectively. In the

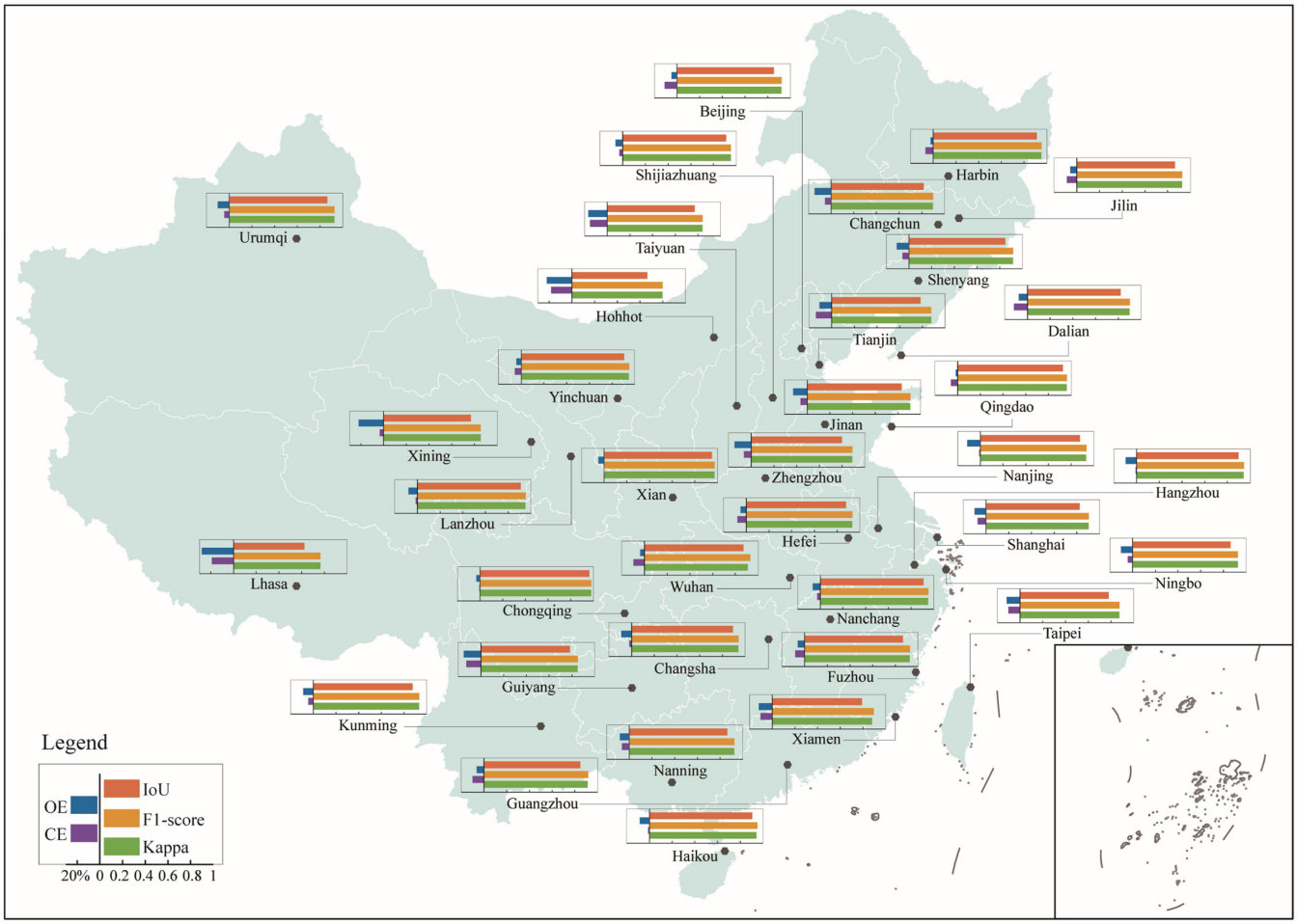

Fig. 8. The extended validation results of urban water extraction with the OTOP method in the major cities of China.

developed cities in Eastern China, such as Beijing, Shanghai, Guangzhou, and other cities with dense high-rise buildings, the OTOP method can accurately distinguish urban water and building shadows, achieving a high water extraction accuracy. The OTOP method also shows a good performance in urban water extraction in some coastal cities such as Dalian, Qingdao, Fuzhou, Xiamen, Haikou, and Taipei. In some inland cities with relatively developed water systems, such as Nanchang, Wuhan, Changsha, and Chongqing, the kappa values of the OTOP method are 0.949, 0.910, 0.941, and 0.980, respectively, and the IoUs are 0.910, 0.872, 0.892, and 0.962, respectively, which are all very high values. The OEs and CEs of the OTOP method are also extremely small values. However, in some cities in Western China, such as Lhasa, Xining, and Hohhot, the comprehensive accuracies of the water extraction are relatively lower, and the OEs are higher. There are fewer water bodies and mainly narrow rivers in these cities, such as the Lhasa River in Lhasa, the Huangshui River in Xining, and the East River in Hohhot, so that there are more mixed pixels in the water areas. The water features of these mixed pixels are not obvious enough to be easily detected, but they are labeled as water according to the expert experience when manually drawing the water masks. In addition to the influence of mixed pixels, too little water can also easily magnify the error indicators in the accuracy assessment.

Furthermore, it can also be found that the OTOP method results in few false detections (low CEs) for urban water extraction in all the cities. This again proves that the OTOP method can effectively distinguish water from building shadows and dark ground surfaces in different urban areas, and it can accurately determine the extent of urban water. The performance of the nine models is also verified by the high accuracy of urban water extraction results for the test data.

V. Discussions

A. Advantages of the Method Combining GEE and MSCNN

In this article, we have proposed the OTOP method for urban water extraction. The OTOP method can not only improve the accuracy of urban water extraction in various environmental backgrounds, but also provide a flexible way to accelerate the efficiency of water extraction, so as to facilitate the related research into long-term and large-scale urban water monitoring.

GEE provides a powerful data storage and data processing platform, which has free access to Landsat data across the entire time series, and it also has the ability to quickly batch-process

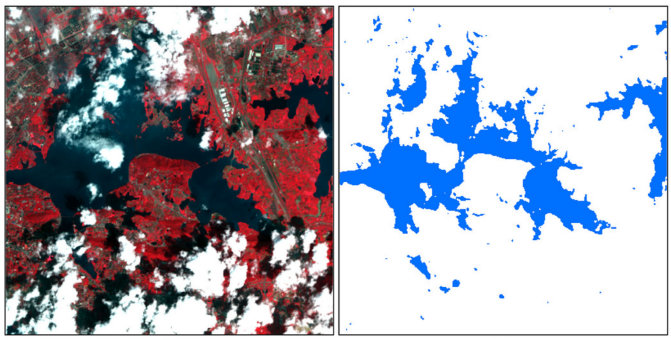

Fig. 9. Part of the water extraction result by the OTOP method for the cloudy Landsat image with path/row 123/039 on September 12, 2017. (a) NIR-R-G false-color display of the original image. (b) Blue color indicates the extracted extent of the water.

large numbers of images, regardless of time and space. Therefore, compared with the other methods of urban water extraction, for which it is necessary to download data for subsequent local processing, the OTOP method can save a lot of time when downloading data and space when storing data. The data processing can also be performed in parallel on GEE, which represents a qualitative leap in processing efficiency.

The classification accuracy of the OTOP method also shows an improvement compared with the traditional water extraction methods already encapsulated on GEE, and there is no need for additional data or separate detection procedures to remove the noise from shadows and dark surfaces. Our experimental data were selected from the Landsat images of 36 cities in different regions of China, which were deliberately chosen to cover different urban water types and urban surface features. If there are some clouds/cloud shadows in the image, the OTOP method can also accurately distinguish water (Fig. 9). Therefore, the OTOP method can achieve a higher precision than the existing traditional water extraction methods on GEE, and it has strong robustness for different types of water extraction in different urban environments. MNDWI and RF may achieve a higher accuracy by adjusting the thresholds or changing the combinations of feature variables. But this will have strong subjective consciousness and require expert experience, as well as a lot of time, and it is not easily extended to large-scale automated application.

Compared with the latest deep learning function implemented on GEE with the TensorFlow framework, the OTOP method has unique advantages. The realization of the existing deep learning function on GEE provides a very convenient approach for scientific research, but it is reliant on the three intermediate platforms of Google Cloud Storage, Google Colaboratory, and AI Platform. When the usage of Google Storage exceeds the specific limits, or when using the Google AI platform to train models and obtain predictions in the cloud, the cost is the factor that must be considered for some studies. As for the proposed OTOP method, the training of the network is done offline, and the powerful computing performance of GEE is sufficient for the part that needs to be processed online, so that the whole process is free. In addition, the OTOP method is not limited by the TensorFlow framework for the programming language and the building style of the network model, so that it is more flexible and free to build the preferred deep learning model. The previously trained deep learning models can also be applied directly on GEE, without being reimplemented in TensorFlow.

In summary, the combination of GEE and MSCNN does not require us to make many subjective decisions affecting the accuracy of the classification, and it also maintains the advantage of the high accuracy of urban water extraction with MSCNN. There is no need to take into account the download of massive data or the requirement for high-performance computing equipment. We have also provided a more flexible way to utilize deep learning models on GEE. The proposed OTOP method can be used to study the characteristics of urban water changes under the context of urbanization in China. It is also possible to apply the idea of the OTOP method to other studies of land-use classification.

B. Further Improvements

Although the OTOP method achieved satisfactory results in this study, there are still several problems. First, due to the limited spatial resolution of Landsat images, most of the edge pixels of water cover a relatively large area which may be composed of water and non-water objects [55]. The OTOP method tends to classify the mixed pixels at the edges of larger water areas as water during the urban water extraction, which is one of the major reasons for the slight misdetection of water pixels in the predicted results (Figs. 4 and 6). This problem could be solved by adding more accurate samples of edge pixels to the training data. In addition, because of the characteristic of the convolution operations, the OTOP method is slightly inferior to the pixel-based water extraction method in terms of the fineness of the water detection. Finally, the training data we selected for the offline training of the MSCNN model were the artificially drawn water masks of Landsat images of China, so the model parameters may be more suitable for the mapping of urban water in Chinese cities. But there are more urban areas with other urban surface characteristics in the world. If we wanted to make the OTOP method applicable globally, it would be necessary to include more training data from different urban areas, to make the use of OTOP more accurate and convincing.

VI. Conclusion

Urban water mapping is very important for urban management and planning. In this article, we have proposed a new method combining GEE with a CNN for urban water extraction, which is called the OTOP method, to facilitate the study of long-term and large-scale urban water change detection. The method involves training a complete MSCNN model offline, and then extracting water in the urban areas on GEE using the trained model parameters. Such a combination can not only give full play to the advantages of GEE, which is specifically designed to manage big data, but also provide a more flexible way to use deep learning models on GEE to improve the accuracy of water extraction. In addition, the OTOP method only requires the six bands of Landsat images as input to separate water

and non-water, and the multiscale feature fusion module in MSCNN can help to keep more information while considering the context during pixel-by-pixel classification. There is no need to manually select thresholds or apply other artificially defined rules in different regions and conditions, or to rely on rich prior knowledge. The results of the comparative experiments with the traditional MNDWI and RF methods on GEE for Changchun, Wuhan, Kunming, and Guangzhou showed that the OTOP method performs better than the other methods. It can effectively suppress the noise from building shadows and other dark surfaces in urban areas while ensuring accurate detection of urban water. In the extended validation for 32 other major cities in China, the high accuracy of urban water extraction with the OTOP method suggests that it also has strong universality, and is suitable for water extraction at different times in different urban areas. Therefore, the OTOP method can meet the requirements for accuracy, automation, and wide application.

APPENDIX

The code of the online prediction part of OTOP and the list of Landsat data used in the experiment can be viewed at http://sendimage.whu.edu.cn/en/resources/, which also includes the model parameters of the offline MSCNN.

ACKNOWLEDGMENT

The authors would like to thank the editors and anonymous reviewers for their valuable suggestions.

REFERENCES

[1] P. Gober *et al.*, "Using watered landscapes to manipulate urban heat island effects: How much water will it take to cool phoenix?," *J. Am. Plan. Assoc.*, vol. 76, no. 1, pp. 109–121, 2009.

[2] T. D. Fletcher, H. Andrieu, and P. Hamel, "Understanding, management and modelling of urban hydrology and its consequences for receiving waters: A state of the art," *Adv. Water Res.*, vol. 51, pp. 261–279, 2013.

[3] N. Du, H. Ottens, and R. Sliuzas, "Spatial impact of urban expansion on surface water bodies—A case study of Wuhan, China," *Landscape Urban Planning*, vol. 94, no. 3–4, pp. 175–185, 2010.

[4] C. Xie, X. Huang, L. Wang, X. Fang, and W. Liao, "Spatiotemporal change patterns of urban lakes in China's major cities between 1990 and 2015," *Int. J Digit. Earth*, vol. 11, no. 11, pp. 1085–1102, 2017.

[5] W. D. Shuster, J. Bonta, H. Thurston, E. Warnemuende, and D. R. Smith, "Impacts of impervious surface on watershed hydrology: A review," *Urban Water J.*, vol. 2, no. 4, pp. 263–275, 2005.

[6] Y. N. Zhou, J. Luo, Z. Shen, X. Hu, and H. Yang, "Multiscale water body extraction in urban environments from satellite images," *IEEE J. Sel. Topics Appl. Earth Observ. Remote Sens.*, vol. 7, no. 10, pp. 4301–4312, Oct. 2014.

[7] Y. Wu, M. Li, L. Guo, H. Zheng, and H. Zhang, "Investigating water variation of lakes in Tibetan Plateau using remote sensed data over the past 20 years," *IEEE J. Sel. Topics Appl. Earth Observ. Remote Sens.*, vol. 12, no. 7, pp. 2557–2564, Jul. 2019.

[8] S. K. McFeeters, "The use of the normalized difference water index (NDWI) in the delineation of open water features," *Int. J. Remote Sens.*, vol. 17, no. 7, pp. 1425–1432, 1996.

[9] H. Xu, "A study on information extraction of water body with the modified normalized difference water index (MNDWI)," *J. Remote Sens.*, vol. 9, no. 5, pp. 589–595, 2005.

[10] G. L. Feyisa, H. Meilby, R. Fensholt, and S. R. Proud, "Automated water extraction index: A new technique for surface water mapping using Landsat imagery," *Remote Sens. Environ.*, vol. 140, pp. 23–35, 2014.

[11] A. Fisher, N. Flood, and T. Danaher, "Comparing landsat water index methods for automated water classification in eastern Australia," *Remote Sens. Environ.*, vol. 175, pp. 167–182, 2016.

[12] L. Lian and J. Chen, "Spatial-temporal change analysis of water area in Pearl river delta based on remote sensing technology," *Procedia Environ. Sci.*, vol. 10, pp. 2170–2175, 2011.

[13] F. Sun, W. Sun, J. Chen, and P. Gong, "Comparison and improvement of methods for identifying waterbodies in remotely sensed imagery," *Int. J. Remote Sens.*, vol. 33, no. 21, pp. 6854–6875, 2012.

[14] L. Jiang and R. M. Narayanan, "A shape-based approach to change detection of lakes using time series remote sensing images," *IEEE Trans. Geosci. Remote Sens.*, vol. 41, no. 11, pp. 2466–2477, Nov. 2003.

[15] C. Qiao, J. Luo, Y. Sheng, Z. Shen, Z. Zhu, and D. Ming, "An adaptive water extraction method from remote sensing image based on NDWI," *J. Indian Soc. Remote Sens.*, vol. 40, no. 3, pp. 421–433, 2011.

[16] F. Sun, Y. Zhao, P. Gong, R. Ma, and Y. Dai, "Monitoring dynamic changes of global land cover types: Fluctuations of major lakes in China every 8 days during 2000–2010," *Chin. Sci. Bull.*, vol. 59, no. 2, pp. 171–189, 2013.

[17] Y. Deng *et al.*, "Spatio-temporal change of lake water extent in Wuhan Urban Agglomeration based on Landsat images from 1987 to 2015," *Remote Sens.*, vol. 9, no. 3, 2017, Art. no. 270.

[18] Y. Sui, D. Fu, X. Wang, and F. Su, "Surface water dynamics in the North America Arctic based on 2000–2016 landsat data," *Water*, vol. 10, no. 7, 2018, Art. no. 824.

[19] C. Wang, M. Jia, N. Chen, and W. Wang, "Long-term surface water dynamics analysis based on Landsat imagery and the Google Earth Engine platform: A case study in the middle yangtze river basin," *Remote Sens.*, vol. 10, no. 10, 2018, Art. no. 1635.

[20] L. Zhang, G.-S. Xia, T. Wu, L. Lin, and X. C. Tai, "Deep learning for remote sensing image understanding," *J. Sens.*, vol. 2016, pp. 1–2, 2016.

[21] X. X. Zhu *et al.*, "Deep learning in remote sensing: A comprehensive review and list of resources," *IEEE Geosci. Remote Sens. Mag.*, vol. 5, no. 4, pp. 8–36, Dec. 2017.

[22] L. Ma, Y. Liu, X. Zhang, Y. Ye, G. Yin, and B. A. Johnson, "Deep learning in remote sensing applications: A meta-analysis and review," *ISPRS J. Photogramm. Remote Sens.*, vol. 152, pp. 166–177, 2019.

[23] F. Isikdogan, A. C. Bovik, and P. Passalacqua, "Surface water mapping by deep learning," *IEEE J. Sel. Topics Appl. Earth Observ. Remote Sens.*, vol. 10, no. 11, pp. 4909–4918, Nov. 2017.

[24] L. Yu, Z. Wang, S. Tian, F. Ye, J. Ding, and J. Kong, "Convolutional neural networks for water body extraction from Landsat imagery," *Int. J. Comput. Intell. Appl.*, vol. 16, no. 1, 2017, Art. no. 1750001.

[25] Y. Chen, R. Fan, X. Yang, J. Wang, and A. Latif, "Extraction of urban water bodies from high-resolution remote-sensing imagery using deep learning," *Water*, vol. 10, no. 5, 2018, Art. no. 585.

[26] W. Fang *et al.*, "Recognizing global reservoirs from Landsat 8 images: A deep learning approach," *IEEE J. Sel. Topics Appl. Earth Observ. Remote Sens.*, vol. 12, no. 9, pp. 3168–3177, Sep. 2019.

[27] N. Gorelick, M. Hancher, M. Dixon, S. Ilyushchenko, D. Thau, and R. Moore, "Google Earth Engine: Planetary-scale geospatial analysis for everyone," *Remote Sens. Environ.*, vol. 202, pp. 18–27, 2017.

[28] L. Kumar and O. Mutanga, "Google Earth Engine applications since inception: Usage, trends, and potential," *Remote Sens.*, vol. 10, no. 10, 2018, Art. no. 1509.

[29] M. C. Hansen *et al.*, "High-resolution global maps of 21st-century forest cover change," *Science*, vol. 850, pp. 2011–2014, Nov. 2013.

[30] N. N. Patel *et al.*, "Multitemporal settlement and population mapping from Landsat using Google Earth Engine," *Int. J. Appl. Earth Observ. Geoinf.*, vol. 35, pp. 199–208, 2015.

[31] A. R. Joshi *et al.*, "Tracking changes and preventing loss in critical tiger habitat," *Sci. Adv.*, vol. 2, no. 4, 2016, Art. no. e1501678.

[32] H. Huang *et al.*, "Mapping major land cover dynamics in Beijing using all landsat images in Google Earth Engine," *Remote Sens. Environ.*, vol. 202, pp. 166–176, 2017.

[33] J. Xiong *et al.*, "Automated cropland mapping of continental Africa using Google Earth Engine cloud computing," *ISPRS J. Photogramm. Remote Sens.*, vol. 126, pp. 225–244, 2017.

[34] J. F. Pekel, A. Cottam, N. Gorelick, and A. S. Belward, "High-resolution mapping of global surface water and its long-term changes," *Nature*, vol. 540, no. 7633, pp. 418–422, 2016.

[35] Z. Tang *et al.*, "Assessing Nebraska Playa wetland inundation status during 1985–2015 using Landsat data and Google Earth Engine," *Environ. Monit. Assess.*, vol. 188, no. 12, 2016, Art. no. 654.

[36] Z. Zou *et al.*, "Continued decrease of open surface water body area in Oklahoma during 1984–2015," *Sci. Total Environ.*, vol. 595, pp. 451–460, 2017.

[37] F. Chen, M. Zhang, B. Tian, and Z. Li, "Extraction of Glacial lake outlines in tibet plateau using Landsat 8 imagery and Google Earth Engine," *IEEE J. Sel. Topics Appl. Earth Observ. Remote Sens.*, vol. 10, no. 9, pp. 4002–4009, Sep. 2017.
[38] A. Hamida *et al.*, "Deep learning for semantic segmentation of remote sensing images with rich spectral content," in *Proc. IEEE Int. Geosci. Remote Sens. Symp.*, 2017, pp. 2569–2572.
[39] C. Robinson, F. Hohman, and B. Dilkina, "A deep learning approach for population estimation from satellite imagery," in *Proc. 1st ACM SIGSPATIAL Workshop Geospatial Humanities*, 2017, pp. 47–54.
[40] T. Zhang and H. Tang, "Built-up area extraction from Landsat 8 images using convolutional neural networks with massive automatically selected samples," in *Proc. Chinese Conf. Pattern Recognit. Comput. Vision*, 2018, pp. 492–504.
[41] C. Verpoorter, T. Kutser, and L. Tranvik, "Automated mapping of water bodies using Landsat multispectral data," *Limnol. Oceanogr. Methods*, vol. 10, no. 12, pp. 1037–1050, 2012.
[42] M. G. Tulbure and M. Broich, "Spatiotemporal dynamic of surface water bodies using Landsat time-series data from 1999 to 2011," *ISPRS J. Photogramm. Remote Sens.*, vol. 79, pp. 44–52, 2013.
[43] K. Rokni, A. Ahmad, A. Selamat, and S. Hazini, "Water feature extraction and change detection using multitemporal Landsat imagery," *Remote Sens.*, vol. 6, no. 5, pp. 4173–4189, 2014.
[44] P. Wu *et al.*, "Spatiotemporal analysis of water area annual variations using a Landsat time series: A case study of nine plateau lakes in Yunnan province, China," *Int. J. Remote Sens.*, vol. 37, no. 24, pp. 5826–5842, 2016.
[45] N. Mueller *et al.*, "Water observations from space: Mapping surface water from 25 years of landsat imagery across Australia," *Remote Sens. Environ.*, vol. 174, pp. 341–352, 2016.
[46] L. Yue, H. Shen, W. Yu, and L. Zhang, "Monitoring of historical glacier recession in yulong mountain by the integration of multisource remote sensing data," *IEEE J. Sel. Topics Appl. Earth Observ. Remote Sens.*, vol. 11, no. 2, pp. 388–400, Feb. 2018.
[47] J. G. Masek *et al.*, "A landsat surface reflectance dataset for North America, 1990–2000," *IEEE Geosci. Remote Sens. Lett.*, vol. 3, no. 1, pp. 68–72, Jan. 2006.
[48] E. Vermote, C. Justice, M. Claverie, and B. Franch, "Preliminary analysis of the performance of the Landsat 8/OLI land surface reflectance product," *Remote Sens. Environ.*, vol. 185, pp. 46–56, 2016.
[49] Z. Li, H. Shen, Q. Cheng, Y. Liu, S. You, and Z. He, "Deep learning based cloud detection for medium and high resolution remote sensing images of different sensors," *ISPRS J. Photogramm. Remote Sens.*, vol. 150, pp. 197–212, 2019.
[50] G. Mateo-García, L. Gómez-Chova, J. Amorós-López, J. Muñoz-Marí, and G. Camps-Valls, "Multitemporal cloud masking in the Google Earth Engine," *Remote Sens.*, vol. 10, no. 7, 2018, Art. no. 1079.
[51] P. O. Gislason, J. A. Benediktsson, and J. R. Sveinsson, "Random forests for land cover classification," *Pattern Recognit. Lett.*, vol. 27, no. 4, pp. 294–300, 2006.
[52] N. Otsu, "A threshold selection method from gray-level histograms," *IEEE Trans. Syst. Man Cybern.*, vol. 9, no. 1, pp. 62–66, Jan. 1979.
[53] Q. Zhang and C. Xiao, "Cloud detection of RGB color aerial photographs by progressive refinement scheme," *IEEE Trans. Geosci. Remote Sens.*, vol. 52, no. 11, pp. 7264–7275, Nov. 2014.
[54] R. M. Haralick, K. Shanmugam, and I. H. Dinstein, "Textural features for image classification," *IEEE Trans. Syst. Man Cybern.*, vol. SMC-3, no. 6, pp. 610–621, Nov. 1973.
[55] M. Feng, J. O. Sexton, S. Channan, and J. R. Townshend, "A global, high-resolution (30-m) inland water body dataset for 2000: First results of a topographic–spectral classification algorithm," *Int. J. Digit. Earth*, vol. 9, no. 2, pp. 113–133, 2015.

Yudie Wang received the B.S. degree in surveying and mapping engineering from the China University of Geosciences, Wuhan, China, in 2017. She is currently working toward the M.S. degree at the State Key Laboratory of Information Engineering in Surveying, Mapping and Remote Sensing, Wuhan University, Wuhan, China.

Her research interests include remote sensing image processing and remote sensing application.

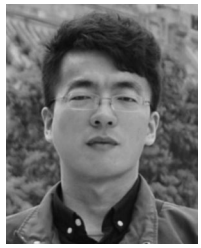

Zhiwei Li received the B.S degree in geo-information science and technology from the China University of Geosciences, Wuhan, China, in 2015. He is currently working toward the Ph.D. degree at the School of Resource and Environmental Sciences, Wuhan University, Wuhan, China.

He is currently working on projects of cloud detection and removal in multisource satellite images for land resources survey. His research interests include cloud detection and removal, deep learning, and remote sensing applications.

Chao Zeng received the B.S. degree in resources-environment and urban–rural planning management, the M.S. degree in surveying and mapping engineering, and the Ph.D. degree in photogrammetry and remote sensing from the Wuhan University, Wuhan, China, in 2009, 2011, and 2014, respectively.

He was a Postdoctoral Researcher with the Department of Hydraulic Engineering, Tsinghua University, Beijing, China. Currently, he is with the School of Resource and Environmental Sciences, Wuhan University. His current research interests include remote sensing image processing, and hydrological remote sensing applications.

Gui-Song Xia (Senior Member, IEEE) received the Ph.D. degree in image processing and computer vision from the CNRS LTCI, Télécom ParisTech, Paris, France, in 2011.

From 2011 to 2012, he was a Postdoctoral Researcher with the Centre de Recherche en Mathmatiques de la Decision, CNRS, Paris-Dauphine University, Paris, France. He has also been a Visiting Scholar with the Department of Mathematics and Applications (DMA), École Normale Suprieure (ENS-Paris), Paris, for two months in 2018. He is currently a Full Professor of Computer Vision and Photogrammetry with the Wuhan University, Wuhan, China. His research interests include mathematical modeling of images and videos, structure from motion, perceptual grouping, and remote sensing imaging.

Dr. Xia serves on the Editorial Boards for the journals *Pattern Recognition*, *Signal Processing: Image Communications*, and *EURASIP Journal on Image and Video Processing*.

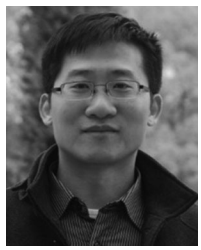

Huanfeng Shen (Senior Member, IEEE) received the B.S. degree in surveying and mapping engineering and the Ph.D. degree in photogrammetry and remote sensing from the Wuhan University, Wuhan, China, in 2002 and 2007, respectively.

In 2007, he joined the School of Resource and Environmental Sciences, Wuhan University, where he is currently a Luojia Distinguished Professor. He has been supported by several talent programs, such as the Youth Talent Support Program of China in 2015, the China National Science Fund for Excellent Young Scholars in 2014, and the New Century Excellent Talents by the Ministry of Education of China in 2011. He has published more than 100 research papers. His research interests include image quality improvement, remote sensing mapping and application, data fusion and assimilation, and regional and global environmental changes.

Dr. Shen is currently a member of the Editorial Board of the *Journal of Applied Remote Sensing*.